In situ process monitoring in selective laser sintering using optical coherence tomography

Michael R. Gardner
Adam Lewis
Jongwan Park
Austin B. McElroy
Arnold D. Estrada
Scott Fish
Joseph J. Beaman
Thomas E. Milner

SPIE.

In situ process monitoring in selective laser sintering using optical coherence tomography

Michael R. Gardner,[a,*] **Adam Lewis,**[b] **Jongwan Park,**[a] **Austin B. McElroy,**[a] **Arnold D. Estrada,**[a] **Scott Fish,**[c] **Joseph J. Beaman,**[c] **and Thomas E. Milner**[a]
[a]The University of Texas at Austin, Department of Biomedical Engineering, Austin, Texas, United States
[b]The University of Texas at Austin, McKetta Department of Chemical Engineering, Austin, Texas, United States
[c]The University of Texas at Austin, Department of Mechanical Engineering, Austin, Texas, United States

Abstract. Selective laser sintering (SLS) is an efficient process in additive manufacturing that enables rapid part production from computer-based designs. However, SLS is limited by its notable lack of *in situ* process monitoring when compared with other manufacturing processes. We report the incorporation of optical coherence tomography (OCT) into an SLS system in detail and demonstrate access to surface and subsurface features. Video frame rate cross-sectional imaging reveals areas of sintering uniformity and areas of excessive heat error with high temporal resolution. We propose a set of image processing techniques for SLS process monitoring with OCT and report the limitations and obstacles for further OCT integration with SLS systems. © *2018 Society of Photo-Optical Instrumentation Engineers (SPIE)* [DOI: 10.1117/1.OE.57.4.041407]

1 Background

Additive manufacturing (AM) is a growing field with rapid industrial incorporation. Selective laser sintering (SLS) in particular is a promising technology for manufacturing parts that have been historically difficult to fabricate using classical machining techniques. SLS works by selectively sintering (melting) polymer powder beds layer by layer.[1,2] After a melt pool is formed for the current layer of the part, a new layer of powder is spread over the entire build area, and the process is repeated. A complex part can thus be constructed in a layer-wise manner. The melt pool cools to form the solidified part, and the excess powder is removed.

As SLS parts begin to be incorporated into devices with heavy governmental regulation (e.g., medical, aerospace) and higher performance, there is a need for precise and accurate feedback to inform the process. Monitoring the powder bed throughout the build can provide metrics on the health of the process and the quality of the part.[3] In fact, several techniques have been proposed and adopted for powder bed monitoring: infrared imaging has been used to monitor surface temperature variations that can contribute to part inadequacies,[4] and high-resolution visible wavelength imaging evaluates two-dimensional (2-D) errors in a layer-by-layer geometry both before[5] and after[6,7] the sintering process.

Although these processes monitor each layer of the build, they do not offer subsurface information about the build. Optical coherence tomography (OCT) has recently been proposed to fill this gap. OCT is an optical imaging technique based on low coherence interferometry.[8] OCT, as a light analog to ultrasound, offers wavelength-encoded depth information about a sample with 1- to 20-μm axial resolution. This imaging technique is the standard of care in ophthalmology, where it is used for corneal and retinal imaging, and

cardiology has also widely adopted the use of intravascular OCT for plaque visualization. One area of growth for OCT is in the manufacturing fields; recent publications have reported OCT systems for automobile paint assessment,[9,10] quantitative touch-screen panel analysis,[11] identification of glass defects,[12] and the evaluation of polymer coatings for pharmaceutical pellets.[13]

OCT has been utilized recently to image SLS parts. Guan et al.[14] demonstrated the utility of OCT for *ex situ* analysis of AM parts and discussed the possibility of *in situ* monitoring for polymers, outlining the significant potential for repair techniques, optimization processes, and material conservation. Correspondingly, we have previously reported both *ex situ* analysis and *in situ* implementation of OCT with SLS to illustrate its utility in resolving layers in sintered parts.[15] In related studies, "inline coherent imaging" has been used for process monitoring in selective laser melting (SLM).[16–18] Though quite similar to SLS in many ways, SLM uses metals with significant optical differences when compared with the polymers used in SLS processes. Whereas inline coherent imaging of metals yields surface topology, OCT imaging of polymers yields cross-sectional data for broader analysis potential.

In this paper, we present a thorough analysis of the optical design and recommendations of image processing protocols for video-rate cross-sectional analysis. We also report new findings on the variation of subsurface defects as a function of laser power.

2 Methods and Materials

2.1 *Optical Design*

The SLS optical design (Fig. 1) includes a CO_2 laser (collimated output with a beam diameter of 4.2 mm), a Keplerian telescope for CO_2 beam expansion (1:5.9) and an objective

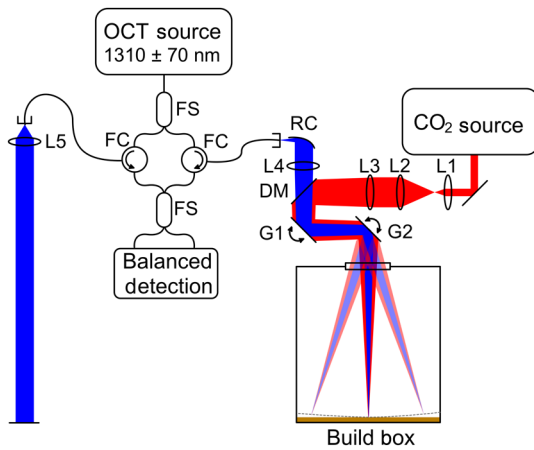*Address all correspondence to: Michael R. Gardner, E-mail: mgardner@utexas.edu

Fig. 1 The SLS + OCT system combines a CO_2 sintering laser (red) with an OCT imaging system (blue). Lens 1 (L1) and lens 2 (L2) are a telescopic beam expander, and lens 3 (L3) is the sintering laser objective. The dichroic mirror (DM) combines the OCT laser source with the CO_2 beam. The OCT system is a fiber-based Mach–Zehnder interferometer. Light from the OCT source is split into reference (left) and sample (right) arms using a fiber coupler (FS). In the reference arm, a fiber circulator (FC) directs light to a reflective collimator (RC) and a mirror before collecting the reflected light. The sample arm uses a reflective collimator and aspheric lens (L4) before the light is combined with the sintering laser. The combined light is directed by a galvanometer mirror pair (G1, G2) before passing through a ZnSe window into the build box. Reflected OCT light is collected, interfered with the reference beam, and detected in a balanced detection scheme.

lens ($f = 750$ mm, NA = 0.015) that focuses the CO_2 light onto the build surface. The beam is directed by a pair of postobjective scanning galvanometers and enters the build chamber through a zinc selenide (ZnSe) window. The maximum area build surface is a circle with radius 109 mm; the radius of the build area is constrained by the size of the ZnSe window. A full description of the SLS system (Laser Additive Manufacturing Pilot System) can be found in Wroe et al.[19] and Fish et al.[20]

The OCT system (Fig. 1) is a fiber-based Mach–Zehnder interferometer design with a swept source laser (1310 nm $\pm$ 70 nm, 100 kHz repetition rate, Axsun). The sample arm light (80%) is collimated to a 12-mm diameter by a reflective collimator and focused by a long focal-length objective lens ($f = 750$ mm, NA = 0.008). The OCT beam is coaligned with the sintering beam using a dichroic mirror and is scanned by the same postobjective scanning galvanometers before the light enters the build chamber through the ZnSe window. Thus, the OCT beam and CO_2 beam are always incident on the same location. The peak sensitivity of the system was experimentally determined to be 98.6 dB with an axial resolution of 11.7 μm, and the system roll-off yielded an imaging range of 3.36 mm (Fig. 2). The OCT beam was incident on the sample with a power of 14.8 mW with a spot size of 3.93 μm (radius) at the focal plane.

2.2 Part Design

To examine the utility of OCT in detecting subsurface changes, an experimental protocol was developed in which the CO_2 beam first sintered two reference points 4-cm apart on a nylon powder bed (2.5 W laser power for
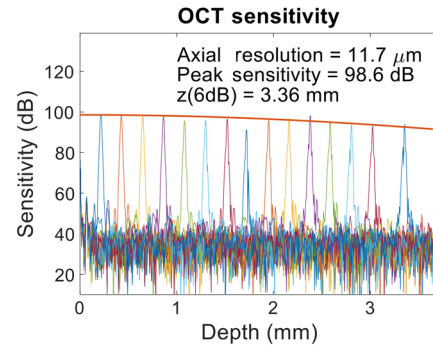

Fig. 2 The OCT system was experimentally determined to have a peak sensitivity of 98.6 dB and an axial resolution of 11.7 μm. By fitting a Gaussian curve to the peak sensitivities at increasing pathlengths, the imaging range (6 dB) was calculated to be 3.36 mm.
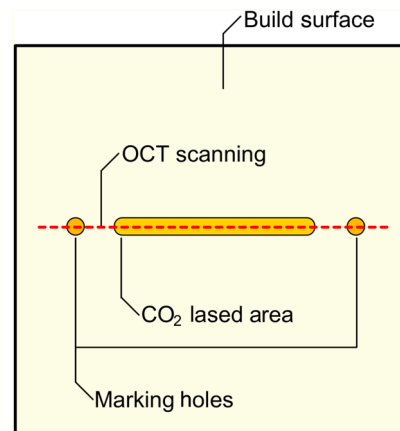

Fig. 3 *En face* view of the build surface. The orange sections indicate areas of nylon sintering; the red dotted line is the OCT beam path.

0.1 s each). These marking holes assisted in identifying the beam location in the resultant OCT image. After these holes were formed, the CO_2 beam sintered a 2.5-cm line directly between the two marking holes. This line was sintered in repeating experiments with a range of laser powers (20%, 40%, 60%, 80%, and 100%). For each experiment, the OCT system captured a series of A-scans at 100 kHz during each of these sintering steps and continued to collect B-scan images of the sintered area for ~3 s after the nylon was sintered to monitor surface and subsurface variation (Fig. 3).

2.3 Image Processing

We process the OCT images using two processing phases to improve the signal-to-noise ratio (SNR)[21] for enhanced image analysis. First, we developed a "second-order interleaving" process. Using this new image processing approach for OCT samples with low light penetration depths, every second data point in each A-scan fringe was taken to form two A-scans fringes from the same A-scan location (1, 3, 5, ..., 1375 and 2, 4, 6, ..., 1376). The resulting two A-scans were averaged to improve the SNR. Because the penetration depth of 1310-nm light in nylon is less than half of our imaging range (3.7 mm), the OCT signal from the build surface was isolated to low-frequency fringe patterns. Thus, though the imaging range is halved by second-order interleaving, the build surface topology was
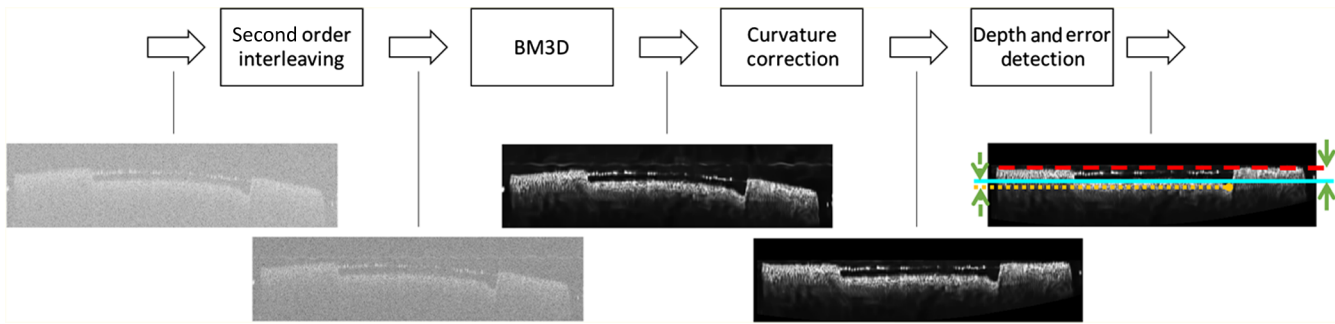
Fig. 4 To obtain the final image and metrics for analysis, a series of image processing steps are performed, including second-order interleaving, BMD3 filter, curvature correction, and depth/error detection.

maintained in both A-scans. After interleaving for improved SNR, the contrast was adjusted and a block matching three-dimensional (BM3D) filter[22] applied.

A second phase corrects the image for the effects of field curvature. The nylon surface in the B-scan exhibits a hyperbolic curve because of postobjective scanning and a fixed reference arm. To correct for this curvature, the top surface of the B-scan is detected using standard edge-detection algorithms and then fit to a second-order polynomial, approximating the hyperbolic curvature close to the turning point. Then, pixels are shifted (with interpolation) to make the top surface horizontal. The bottom surface of the melt pool was found by a second edge-detection algorithm. Finally, the melt pool depth was calculated by the mean distance from the top surface, and the excessive heat error was recorded as the max distance of the melt pool edge from the melt pool mean depth (Fig. 4).

3 Results

The incorporated SLS+OCT design observed subsurface melt pool changes that were previously only inferred by 2-D *en face* imaging and postprocessing analysis. The OCT images reveal the top surface of the nylon powder and the top and bottom surface of the melt pool. The OCT images also show subsurface flaws in the build due to excessive heating.

As the laser power increased from 20% (4.6 W) to 100% (32.5 W), the average melt pool depth increased monotonically from 0.01 to 0.17 mm. Additionally, a defect area of increased melt pool depth was observed at the temporally distal end of the scan (the right edge of the melt pool). This "excessive heat error" (maximum depth as measured from the average melt pool depth) also increased monotonically as a function of laser power from an average of 0.02 to 0.12 mm (Fig. 5 and Video 1).
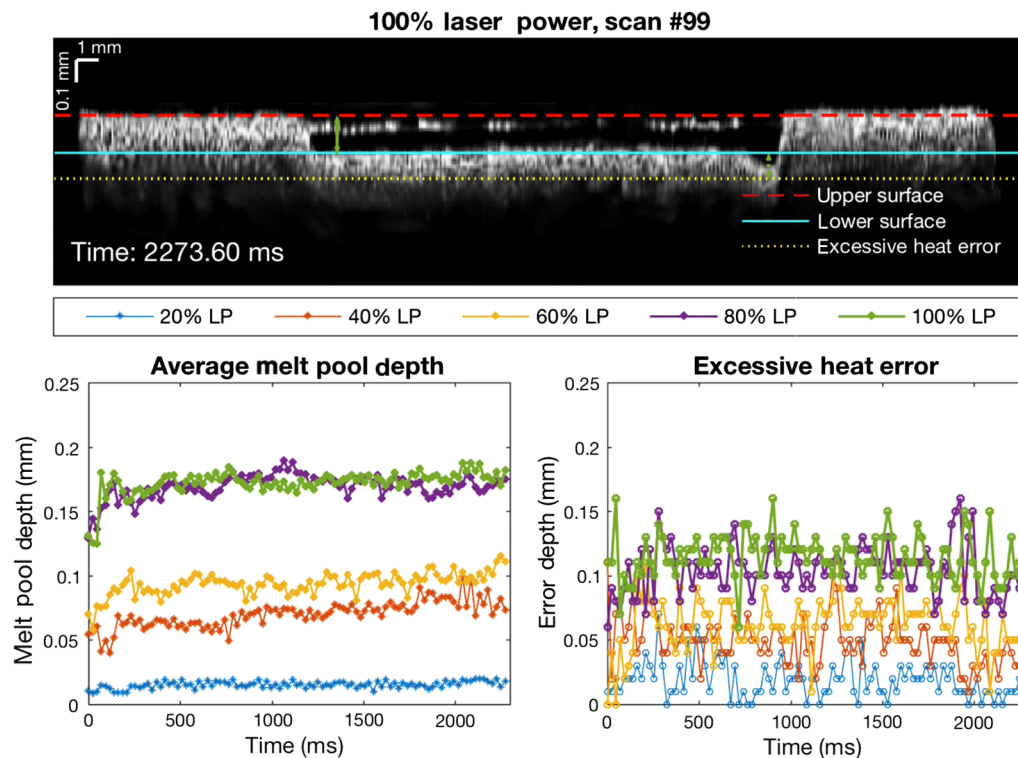

Fig. 5 OCT imaging after sintering reveals a slight upward trend in average melt pool depth with time as the heat diffuses through the powder bed. Also, increasing laser powers create deeper melt pools and larger excessive heat errors on the temporally distal end of the sintering laser sweep (right side) (Video 1, MP4, 23.6 MB [URL: https://doi.org/10.1117/1.OE.57.4.041407.1]).
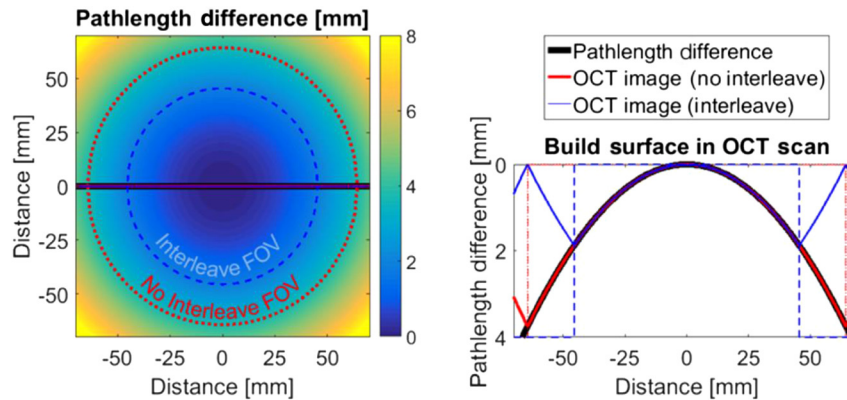
Fig. 6 The imaging range of the OCT system limits the FOV because postobjective scanning hyperbolically varies the path length difference between the flat powder surface and the static reference arm mirror. The FOV and cross-sectional image with no interleaving is pictured by the red lines. The FOV is smaller after interleaving (blue), and the corresponding cross-sectional image exhibits faster aliasing due to down sampling in the *k*-space domain.

4 Discussion

It was anticipated that greater sintering laser powers would yield a deeper melt pool because of a larger temperature gradient. However, as mentioned in the results section, the OCT system detected "excessive heat error" that illustrates the utility of a three-dimensional imaging approach and OCT in particular. Near the right edge of the sintered area a defect area became apparent at low laser powers and increasingly more remarkable at higher laser powers. The defect occurred where the sintering laser was turned off to stop the sintering process. It is probable that this defect is due to a slight dissimilarity in the amount of energy deposited into the powder (excessive heat), either by a sudden increase in laser power as the laser is turned off, or more likely, a deceleration, or lingering of the galvanometer scanning at the "turn off" location due to galvanometer constraints. With these images as feedback, laser power could be responsively varied to minimize this excessive heat error.

Field curvature limited the build area for OCT imaging. Due to the OCT system's imaging depth, any surface that had a pathlength difference of >3.7 mm was aliased in the OCT fringe as a low-frequency component and thus unreliable for interpretation. With the field curvature induced by postobjective scanning and the OCT system's imaging depth, the build area is limited to a circle with a 64-mm radius, where the center point appears as the shortest pathlength difference (distance 0, 0 in Fig. 6) and the edges are the longest pathlength difference. Down-sampling for second-order interleaving further limited the field of view to a circle with 45-mm radius (blue inner circle in Fig. 6).

In the present iteration, the OCT beam and the sintering beam are coaligned and share the same galvanometer mirrors. This limits any live imaging to the current sintering location. The experiment performed in this study revealed postsintering time points by scanning the galvanometer mirrors across the sintered area after the sintering laser turned off. However, including a "fast scan" galvanometer in the OCT beam path before the shared galvanometers would enable imaging of areas around the instantaneous location of the sintering beam.

Future studies could advance the utility of SLS + OCT by recording the absolute temperature of the polymer surface during the build. Although the LAMPS system had been previously equipped with an IR camera for temperature monitoring,[19,23] the reported OCT system used the same dichroic and thus precluded simultaneous IR and OCT monitoring. With an additional dichroic, the correlation of OCT data with the absolute temperature could prove useful in building a database of common depth-resolved errors with certain surface temperature profiles.

Rapid, real-time processing is necessary for a live feedback mechanism and responsive defect correction. Real-time processing was not the aim of this study, but this work lays out potential processing pathways for interpreting OCT data for such mechanisms.

5 Conclusions

An OCT imaging system was incorporated into an SLS machine. The data show that OCT can detect subsurface defects with micron resolution. We found that, as expected, higher laser powers produced a deeper melt pool. Moreover, the OCT system showed that an excessive heating error produces increasingly larger build faults as the laser is turned off. Additionally, a series of image processing steps including a new technique called "interleaving" offer enhancement for long focal-length OCT imaging of powder beds for AM.

References

1. J. J. Beaman and C. R. Deckard, "Selective laser sintering with assisted powder handling," U.S. Patent No. US4938816 A (1990).
2. C. R. Deckard, "Apparatus for producing parts by selective sintering," U.S. Patent No. US4863538 A (1989).
3. T. G. Spears and S. A. Gold, "In-process sensing in selective laser melting (SLM) additive manufacturing," *Integr. Mater. Manuf. Innov.* **5**(1), 2 (2016).

4. A. Wegner and G. Witt, "Process monitoring in laser sintering using thermal imaging," in *Proc. of the 22nd Int. SFF Symp.-An Additive Manufacturing Conf.*, pp. 8–10 (2011).
5. T. Craeghs et al., "Online quality control of selective laser melting," in *Proc. of the 22nd Int. SFF Symp.-An Additive Manufacturing Conf.*, Austin, pp. 212–226 (2011).
6. S. Kleszczynski et al., "Error detection in laser beam melting systems by high resolution imaging," in *Proc. of the 23rd Int. SFF Symp. An Additive Manufacturing Conf.*, Austin (2012).
7. A. L. Cooke and S. P. Moylan, "Process intermittent measurement for powder-bed based additive manufacturing," in *Proc. of the 22nd Int. SFF Symp. An Additive Manufacturing Conf.*, Austin, pp. 8–10 (2011).
8. D. Huang et al., "Optical coherence tomography," *Science* **254**(5035), 1178–1181 (1991).
9. Y. Dong et al., "Non-destructive characterization of automobile car paints using terahertz pulsed imaging and infrared optical coherence tomography," in *40th Int. Conf. on Infrared, Millimeter, and Terahertz waves (IRMMW-THz)*, pp. 1–2, IEEE (2015).
10. J. Zhang et al., "Non-destructive analysis of flake properties in automotive paints with full-field optical coherence tomography and 3D segmentation," *Opt. Express* **25**(16), 18614–18628 (2017).
11. N. H. Cho et al., "Quantitative assessment of touch-screen panel by non-destructive inspection with three-dimensional real-time display optical coherence tomography," *Opt. Lasers Eng.* **68**, 50–57 (2015).
12. Z. Chen et al., "Identification of surface defects on glass by parallel spectral domain optical coherence tomography," *Opt. Express* **23**(18), 23634–23646.
13. C. Li et al., "Non-destructive evaluation of polymer coating structures on pharmaceutical pellets using full-field optical coherence tomography," *J. Pharm. Sci.* **103**(1), 161–166 (2014).
14. G. Guan et al., "Evaluation of selective laser sintering processes by optical coherence tomography," *Mater. Des.* **88**, 837–846 (2015).
15. A. Lewis et al., "In-situ process monitoring and ex-situ part quality assessment of selective laser sintering using optical coherence tomography," in *Proc. of the 27th Int. SFF Symp.-An Additive Manufacturing Conf.*, Austin, pp. 1397–1411 (2016).
16. A. Neef et al., "Low coherence interferometry in selective laser melting," *Phys. Procedia* **56**(Suppl. C), 82–89 (2014).
17. U. Thombansen, A. Gatej, and M. Pereira, "Process observation in fiber laser–based selective laser melting," *Opt. Eng.* **54**(1), 011008 (2015).
18. J. A. Kanko, A. P. Sibley, and J. M. Fraser, "In situ morphology-based defect detection of selective laser melting through inline coherent imaging," *J. Mater. Process. Technol.* **231**, 488–500 (2016).
19. W. W. Wroe et al., "In-situ thermal image correlation with mechanical properties of nylon-12 in SLS," *Rapid Prototyp. J.* **22**(5), 794–800 (2016).
20. S. Fish et al., "A high temperature polymer selective laser sintering testbed for controls research," in *Proc. of the 27th Int. SFF Symp.-An Additive Manufacturing Conf.* (2015).
21. R. Leitgeb, C. K. Hitzenberger, and A. F. Fercher, "Performance of fourier domain vs. time domain optical coherence tomography," *Opt. Express* **11**(8), 889–894 (2003).
22. K. Dabov et al., "Image denoising with block-matching and 3D filtering," *Proc. SPIE* **6064**, 606414 (2006).
23. T. Phillips et al., "In-situ laser control method for polymer selective laser sintering (SLS)," in *Proc. of the 27th Int. SFF Symp.-An Additive Manufacturing Conf.*, Austin, pp. 1381–1396 (2016).

Michael R. Gardner is a PhD candidate in biomedical engineering at the University of Texas at Austin. His research is related to optical imaging and image processing.

Biographies for the other authors are not available.